www.ietdl.org

Published in IET Microwaves, Antennas & Propagation
Received on 26th November 2012
Revised on 16th April 2013
Accepted on 13th May 2013
doi: 10.1049/iet-map.2012.0685

ISSN 1751-8725

Inkjet-printed antennas, sensors and circuits on paper substrate

Sangkil Kim[1], Benjamin Cook[1], Taoran Le[1], James Cooper[1], Hoseon Lee[1], Vasileios Lakafosis[1], Rushi Vyas[1], Riccardo Moro[2], Maurizio Bozzi[2], Apostolos Georgiadis[3], Ana Collado[3], Manos M. Tentzeris[1]

[1]*Department of Electrical and Computer Engineering, Georgia Institute of Technology, Atlanta, GA, USA*
[2]*Department of Electrical, Computer and Biomedical Engineering, University of Pavia, Pavia 27100, Italy*
[3]*Centre Tecnologic de Telecomunicacions de Catalunya, CTTC, Castelldefels 08860, Spain*
E-mail: ksangkil3@gatech.edu

Abstract: Inkjet-printing is a very promising technology for the development of microwave circuits and components. Inkjet-printing technology of conductive silver nanoparticles on an organic flexible paper substrate is introduced in this study. The paper substrate is characterised using the T-resonator method. A variety of microwave passive and active devices, as well as complete circuits inkjet-printed on paper substrates are introduced. This work includes inkjet-printed artificial magnetic conductor structures, a substrate integrated waveguide, solar-powered beacon oscillator for wireless power transfer and localisation, energy harvesting circuits and nanocarbon-based gas-sensing materials such as carbon nanotubes and graphene. This study presents an overview of recent advances of inkjet-printed electronics on paper substrate.

1 Introduction

Inkjet-printing technology is a well-known technology for most people as it is one of the most common method of printing in both personal and commercial settings. In the field of electrical engineering, it has been shown that conductive traces can be formed by using a conductive ink. This method of printing has also been shown to be usable for a variety of different substrates in addition to paper, many of which are greatly flexible. The ability to utilise flexible substrates, as well as it being a completely additive method of fabrication, has led many research groups to investigate its properties and applications [1–3]. Beyond the use of flexible substrates, the ever-growing demand for low-cost, environmentally-friendly and flexible wireless device has brought about brilliant progress [4, 5]. Photo paper is an environmentally-friendly material that is coated by photographic emulsion, which is a light-sensitive colloid, similar to gelatin. Different from other flexible substrates like a polyethylene terephthalate (PET) or polyimide, manufacturing process of photo paper's photographic emulsion neither involves harmful chemicals such as phenolic compounds nor releases environmental hormones when it is heated up. In addition, photo paper is recyclable; and wood-free paper exists.

Inkjet-printing technology has emerged as an alternative to conventional fabrication techniques such as etching and milling, since it is both a cost-efficient and an environmentally-friendly method in [6, 7]. Inkjet-printing is a purely additive process, only depositing conductive lines where needs, which does not produce unwanted material, such as in etching and milling where waste chemicals and/or materials are produced. In etching, the waste includes hazardous chemicals, which are required to etch away the unwanted metal, and this waste is to be reprocessed [8]. The inkjet-printing method only uses as much ink as it needs and produces no by-products, unlike the conventional methods. Therefore lots of metals can be saved without extra. A commercially available inkjet printer has a feature size of 50 µm. Silver nanoparticle inks are utilised for printing conductive traces to make sure a good metal conductivity, and thus low ohmic loss is achieved. Silver is used both because of its high conductivity and low oxidation. In addition, the ease for fabrication and prototyping of radio frequency (RF)/wireless circuits, which are a commonality of inkjet printing, is an important aspect of this technology because of its feasibility as a fabrication technology for next generation electronics such as radio frequency identification (RFID), wireless sensors, passive/active flexible circuits and printed capacitors [9].

Selecting the optimal substrates is one of the major issues in order to effectively realise low-cost, flexible inkjet-printed electronics. Paper, owing to its availability and flexibility, has been thoroughly studied and applied to RF applications [4]. As paper is one of the cheapest materials in the world, it is desirable in mass deployment for RFID and wireless sensor networks (WSN). In addition, it is an organic flexible and recyclable substrate. Paper is also desirable because of being easier to print on other popular inkjet-printing substrates, such as

polytetrafluoroethylene (PTFE) and a liquid crystal polymer (LCP). PTFE has a very low surface energy, which lead to pulling and beading of printed inks. LCP, which is a costly material, is easily damaged in the curing process as the ink poses a stress on the LCP and causes wrinkling. The downside of paper is its high loss tangent (tan δ) which becomes a major issue in wireless sensor and other high-Q resonant structures. The cutting edge results of inkjet-printed electronics on the paper substrate such as passive/active antenna, substrate integrated waveguide (SIW), frequency selective surface (FSS), energy scavenging circuit and sensing material utilising graphene and carbon nanotubes (CNTs) are going to be introduced in this paper, and their possible future works are also going to be discussed.

This paper is organised as follows: Section 2 summarises the characteristics of the inkjet-printed silver traces and paper substrate. Section 3 introduces the state-of-the-art inkjet-printed passive/active components, circuits, wireless systems using surface mount devices (SMD) and nanocarbon-based devices. Lastly, future works and conclusion are presented in Sections 4 and 5, respectively.

2 Characterisation of inkjet-printed nanosilver particles and paper

As with any fabrication process used for microwave design, the electrical properties of the substrate, such as the permittivity (ε_r) and loss tangent (tan δ), and properties of the printed metallic nanoparticle inks being used, such as conductivity and metallisation thickness, are essential. These properties along with feature size, gap size and processing factors such as temperature and chemical exposure determine the possible end applications that can use the process. This information is also crucial to accurate modelling and simulation of high-frequency devices. In this section, the electrical characterisation of photo paper using inkjet printing with silver nanoparticles will be discussed and the fabrication parameters will be formulated.

To note, throughout this paper, a silver epoxy is utilised to mount connectors and SMDs on silver traces. Its tensile lap shear strength is larger than 70–140 Kgm cm^2 and shore D hardness is larger than 70 depending on curing temperature.

2.1 Electrical conductivity of inkjet-printed nanosilver particles

One of the major issues of inkjet-printing is characterising the conductivity of printed silver nanoparticles. Silver nanoparticles form an agglomeration of silver particles 10–50 nm in size when they are deposited on the substrate and they are surrounded by a polymer coating, which is used as a dispersant while the particles are in ink form. Upon deposition, the net structures have a low conductive because the particles are suspended in a solvent. A sintering process is required to evaporate the solvent and melt the particles together to achieve high conductivity. The heat sintering is examined in this paper as it is the most common of the methods to sinter metallic nanoparticles. However, other processes such as laser, UV flash lamp and microwave sintering have been demonstrated and utilised [10–12]. Several variables play an important role in the conductivity of the printed structures. Number of ink layers printed, surface roughness of the substrate, sintering temperature and ink properties, such as nanoparticle concentration, are the key factors determining conductivity of printed inks.

Heat sintering is one of the most common methods of annealing or melting nanoparticle inks to form continuous conducting structures. Metallic nanoparticles exhibit a unique property in which their small size decreases their melting point to temperatures as low as 80°C which is important when printing on substrates such as paper and plastic which cannot be handled at high temperatures. To test the conductivity, a series of traces are printed on a paper substrate using 1–5 layers of ink and all printed structures use a 10 pL cartridge with 1024 dpi (20 µm drop spacing). The substrates are then placed in an air-filled oven at atmospheric pressure using different times and temperatures for curing. The resistance of the traces is then measured using the four-point probe method on a cascade probing station. As sintering temperature and number of ink layers printed increases, conductivity increases as shown in previous work [13]. Higher temperature increases conductivity by dissolving more of the solvent and further fusing the silver nanoparticles. Printing more layers helps by increasing the density of particles in a given area so that when melted together, the nanoparticles form less of a porous and more of a uniformly solid structure. More layers, also increases the thickness of the conductive traces, thus increasing the bulk conductance. Fig. 1 shows printed patterns on paper substrate for sheet resistance measurements, and the sheet resistances of widely used silver nanoparticle inks on paper are presented in Fig. 2. Five layers of silver traces were printed using inks from Cabot and UT-Dots, and conductivity variations after 1 h of sintering process at different sintering temperatures were measured (Fig. 2). The impedance is measured in the ohms

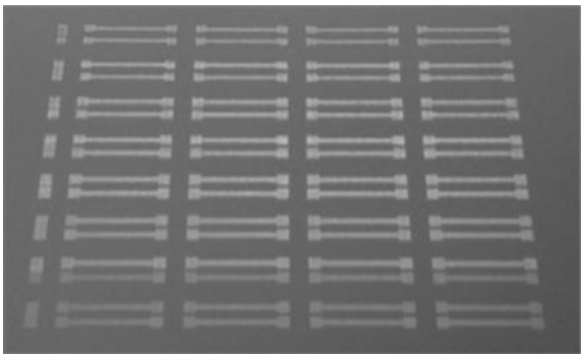

Fig. 1 *Inkjet-printed traces for conductivity measurement*

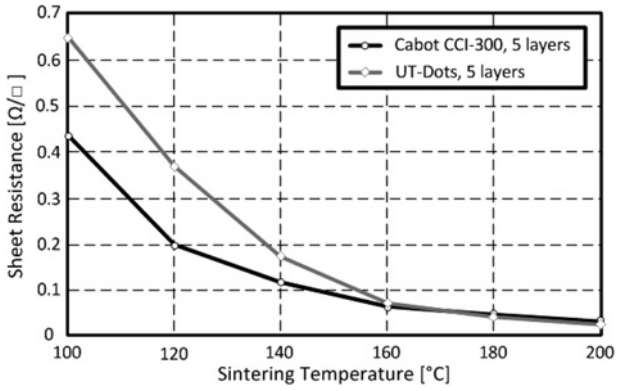

Fig. 2 *Sheet resistance and sintering temperature*

Table 1 Conductivity of printed nanosilver particles [13]

Layers	Conductivity, S/m	
	120°C	200°C
1	0.55×10^6	1.1×10^6
3	1.16×10^6	5.56×10^6
5	2.16×10^6	1.2×10^7

per square standard (Ω/□). In addition, the reported pull-off breaking force of the sintered silver lines on flexible substrates is about 50 N [14] and its Young's modulus is a function of sintering temperature. The reported Young's modulus of the printed silver line is about 5 GPa when the sintering temperature is 150°C and about 52 GPa when the sintering temperature is 200°C [14]. The humidity affects adhesion strength more so than conductivity. The conductivity difference between the printed silver lines on paper substrate in 30 and 53% humidity was only about 2.8%. However, the adhesion strength of the printed silver lines is decreased dramatically when the substrate absorbs moisture. The reported average pull-off strength of the wet flexible substrate is about 21 N, which is much smaller than that of the dry substrate (51 N) [14]. This result suggests that the printed trace is more flexible when it is sintered at lower temperature than the higher temperature.

In order to extract the conductivity from the sheet resistance, the layer thicknesses are needed. As the surface roughness on polymer and organic substrates is higher than the thickness of the conductors, 1–5 layers of ink were printed on glass which has a smooth surface, and then were sintered at 200°C for 1 h. The traces were then measured using a Dekktak profilometer. From the measurement, it is seen that each layer adds approximately 500 nm of thickness to the structure. The thickness of the single layer was about 0.5 µm and five layers was about 2.5 µm. Using the area of the traces along with their resistance yields the conductivity of the sintered nanoparticle inks as shown in the following equation

$$\sigma = \frac{1}{\text{Sheet resistance} \times \int (\text{trace height}) \mathrm{d}x} \tag{1}$$

The following table contains the estimated conductivities for the previously tested structures.

As seen in Table 1, using the correct sintering parameters can lead to conductivities above 10^7, which is only five times lower than bulk silver at 6.4×10^7 S/m. Introducing more printed layers, or sintering at higher temperatures can bring inks even closer to bulk silver conductivities, but at an increased cost. The results from this section prove that silver nanoparticle inks are suitable for implementing microwave frequency structures and antennas.

2.2 Substrates characterisation

The lack of available substrate characterisation data on polymer and organic substrates is a major obstacle in using them for the fabrication of microwave structures. Therefore whenever using a new flexible substrate such as paper the electrical properties must be characterised. Several methods have previously been used to characterise microwave substrates ranging from resonant cavities, transmission line resonators and group velocity measurements of microstrip and co-planar waveguide structures [15]. The T-resonator, while not as common as the ring resonator in characterisation, is much simpler to fabricate as it consists of a microstrip transmission line with an open circuit stub. The structure of the T-resonator is shown in Fig. 3*a*. Owing to the open circuit stub with length d, a null occurs in the transmission whenever d is an odd multiple of a quarter wavelength which is caused by the reflected wave being 180° out of phase once it returns from the open end of the stub, and the width (W) of the resonator corresponds the width of 50 Ω microstrip line [16]. The equation for resonance ($f_{r,n}$) is

$$f_{r,n} = \frac{n\,c}{4(d+k)\sqrt{\varepsilon_{\text{eff},n}}} \tag{2}$$

where n is the resonance index (1, 3, 5, …), c is the speed of light in vacuum, d is the length of the open circuit stub and ε_{eff} is the effective permittivity of the microstrip line. However, owing to the parasitic of the T-junction and fringing fields at the end of the open circuit stub, a correction factor for the length of the stub needs to be incorporated when calculating ε_{eff}. A method for doing this is presented in [16]. Shown in (3), k is the correction factor which includes the junction and open circuit effects on the resonant frequency

$$\varepsilon_{\text{eff},n} = \left(\frac{n\,c}{4(d+k)f_{r,n}}\right)^2 \tag{3}$$

Using the relations of relative to effective permittivity in a microstrip, the permittivity of the substrate can be extracted.

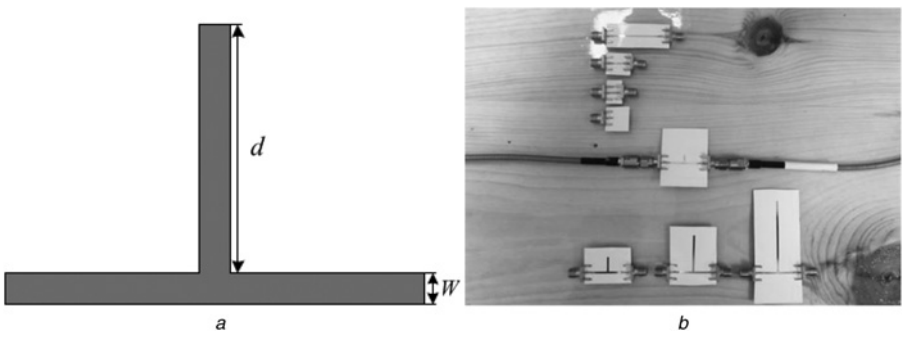

Fig. 3 *Microstrip T-resonator*

a Structure
b Inkjet-printed T-resonators and TRL calibration structures on paper

doi: 10.1049/iet-map.2012.0685

The Q-factor of the resonance peaks can be used to extract the loss tangent of the substrate. The loaded Q-factor is calculated in (4), and then needs to be converted to the unloaded Q-factor (5) which de-embeds the loading caused by the measurement equipment [17].

$$Q_{l-n} = \frac{f_{r,n}}{\mathrm{BW}_{3\,\mathrm{dB}-n}} \tag{4}$$

$$Q_{ul-n} = \frac{Q_{l-n}}{\sqrt{1 - 2 \times 10^{\mathrm{IL}/10}}} \tag{5}$$

In (4), Q_{l-n} is the Q-factor for the nth resonance, $f_{r,n}$ is the resonant frequency and $\mathrm{BW}_{3\,\mathrm{dB}-n}$ is the 3 dB bandwidth at the resonance frequency. In (5), IL is the insertion loss at resonance which is used to de-embed the loading effects. The total losses in the microstrip resonator (6) can then be extracted [18].

$$\begin{aligned}\alpha_{\mathrm{tot},n} &= \alpha_{c,n} + \alpha_{d,n} + \alpha_{r,n} \\ &= \frac{8.686\pi f_{r,n}\sqrt{\varepsilon_{\mathrm{eff},n}}}{cQ_{ul-n}}\left[\frac{\mathrm{dB}}{\mathrm{length\ unit}}\right]\end{aligned} \tag{6}$$

There are a variety of methods to extract conductor and radiation losses, however in this work, Agilent's Line-calc utility is used to subtract these two losses from the total loss leaving only the dielectric losses. The dielectric loss can be directly converted to loss tangent through (7) using standard microstrip loss equations given in [18].

$$\tan\delta = \frac{\alpha_{d,n}\lambda_o\sqrt{\varepsilon_{\mathrm{eff},n}}\left(\varepsilon_{r,n} - 1\right)}{8.686\pi\varepsilon_{r,n}\left(\varepsilon_{\mathrm{eff},n} + 1\right)} \tag{7}$$

The paper-based T-resonator is shown in Fig. 3*b* along with the TRL calibration structures. The stub was designed to have resonances at odd intervals of 1 GHz (1, 3, 5, …), with the intent of measuring the permittivity (ε_r) and loss tangent (tan δ) up to 10 GHz. Although more frequency points would have been better, a lower resonant frequency would require a longer stub which is more difficult to fabricate and can cause more uncertainty in extracting conductor loss. The extraction of the relative permittivity is shown in Fig. 4, and the extraction of the loss tangent (tan δ) is shown in Table 2. The water content of the paper was in the range of 3–8%. The loss tangent (tan δ) is within the reasonable range to previously published data which leads to believe the extracted value was accurate.

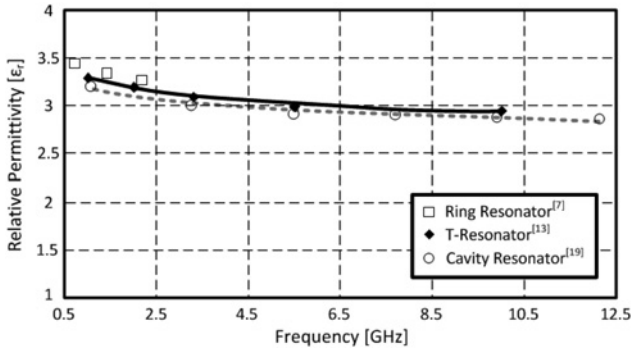

Fig. 4 *Extracted relative permittivity (ε_r)*

Table 2 Extracted loss tangent (tan δ)

	Min	Max
ring resonator [7]	0.053	0.061
T-resonator [13]	0.055	0.065
cavity resonator [19]	0.06	0.07

3 Inkjet-printed passive/active electronics

3.1 Frequency selective surfaces (FSS) and artificial magnetic conductor (AMC) structures on organic and flexible substrate

In the pursuit of more versatile and rugged wireless systems, high impedance surfaces have many applications. Its major advantage is in increased realised gain for antennas, as well as having applications as a surface wave suppressant and beam splitter. In order to cover the applications of these high impedance surfaces, their operation is first covered. This will be followed by a description of two common types of planar high impedance surfaces. Finally the application will be covered.

3.1.1 Construction of FSS and AMC structures: Infinite impedance surfaces and perfect magnetic conductor have yet to be realised. However, constructs exist which yield the same parameters as an infinite impedance surface over a certain bandwidth. One such is the frequency selective surface, or FSS, which can be constructed by the tessellation of a resonant structure, printed or etched in a conductive material, over a two-dimensional (2D) surface [20–22].

FSSs are of great interest because of their ability to be easily printed on sheets of very small thickness (<1 mm). FSS can also be easily manufactured using etching [21], and inkjet printing of silver nanoparticles on organic substrates [22]. The major drawback of FSS, for its use as a back plane reflector for antennas, is that the FSS can easily become detuned by the presence of other materials.

AMC structures are able to work around the issue of detuning. An AMC is similar to an FSS in that it uses a tessellation of a shape across a 2D surface. The difference is that the AMC uses a solid ground plane underneath the 2D surface [23–26]. This prevents interference from nearby materials. The disadvantage is that either the Q-factor of the FSS is greatly increased, the thickness of the AMC becomes much larger than the FSS or the AMC requires the use of vias.

3.1.2 Beam splitter: Realised high impedance surfaces only operate as such over a certain bandwidth. FSS has the unique property that away from the frequency of operation, the FSS begins to appear transparent to transmission electron microscopy (TEM) waves. In the transition from high impedance to transparent, TEM waves are subject to magnitude of reflection coefficients ranging from 0 to 1. At the point where the coefficient is 0.707, half the power incident on the FSS is transmitted through and half the power is reflected back. If the FSS is illuminated at a non-trivial angle of incidence, such as in Fig. 5, half the power would be sent in one direction, whereas half the power would be sent in another direction. In this manner, the FSS could be used as a free space beam splitter. Cooper *et al.* [27] reported the experimental results of the

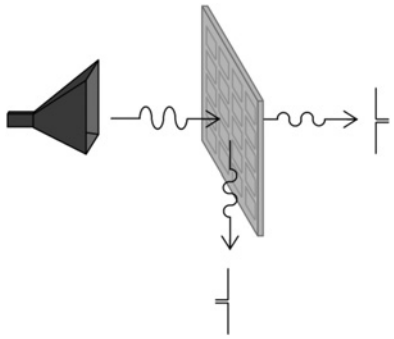

Fig. 5 *FSS being used as a 3 dB beam splitter*

inkjet-printed free space beam splitter. The inkjet-printed FSS operates as a good FSS and splits the wave very well.

3.1.3 Antennas on inkjet-printed AMC plane: Both AMC and FSS are very useful for backing antennas in order to increase the realised gain. Recently, a monopole antenna and dipole antenna were mounted on the inkjet-printed AMC structure (Kim *et al.* [25] and Lee *et al.* [28]). A simple monopole antenna and dipole antenna are placed on top of an inkjet-printed FSS, and a copper sheet is then placed underneath the FSS to form an AMC ground plane (Figs. 6*a* and *b*). These antenna designs are currently being used in the design of wearable antennas. The use of the AMC ground plane as a reflector prevents energy from being radiated into a human body, prevents the presents of a body from detuning the antenna and increases the overall gain of the antenna.

The gain of the monopole antenna with the AMC plane which covers from 2.36 to 2.61 GHz is measured (Fig. 7*a*). It shows the effect of the inkjet-printed AMC structure on the human body very well. About 9 dBi of antenna gain at 2.45 GHz is realised on human body due to the AMC ground plane. The inkjet-printed AMC ground effectively isolate the antenna and the human body which results in relatively high gain on the human body.

For demonstration, the monopole antenna on inkjet-printed AMC plane is integrated with a commercial temperature sensor (Texas Instrument, eZ430-RF2500), and the complete system is mounted on the back of human [29]. For the monopole antenna, the transmitter was mounted on the chest, and the communication distance was defined when the receiver lost signal from the transmitter. The communication range of the on-body sensor module with a conventional chip antenna was 18.3 m; with an inkjet-printed meandered monopole antenna it was 29.5 m; and with the proposed antenna it was 82.8 m (Fig. 8*a*). For the dipole RFID antenna, it was attached both to a metal surface and to a human body. The Impinj Speedway Reader was used to measure the packet loss of the tag on AMC. The packet loss can be defined as the ratio between the number of lost replies from the tag to the total number of performed interrogations. Like the monopole antenna's case, communication range of the tag has been increased because the tag on AMC can be read up to 2.5 and 4.5 m when attached to metal and human body, respectively.

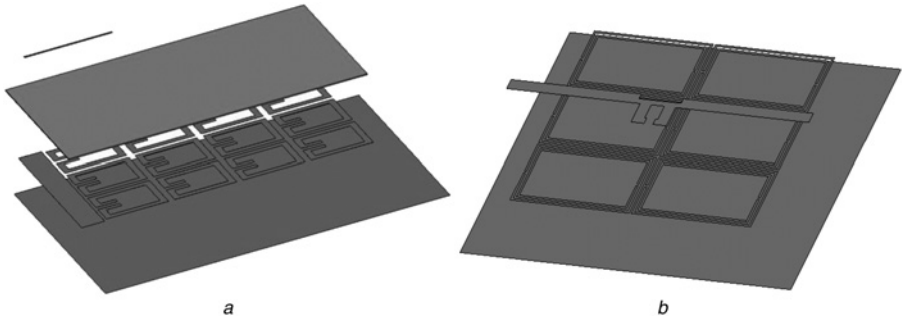

Fig. 6 *Copper sheet is then placed underneath the FSS to form an AMC ground plane*

a Monopole antenna
b dipole RFID antenna on AMC

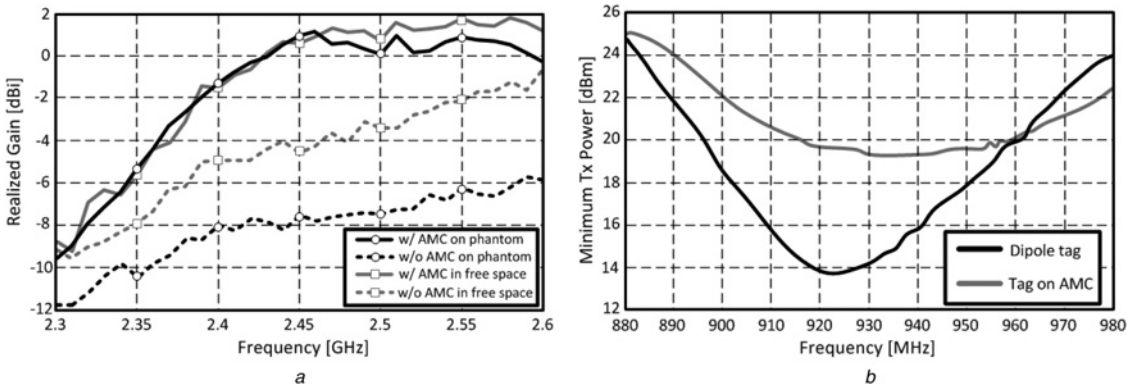

Fig. 7 *Gain of the monopole antenna with the AMC plane*

a Realised gain of monopole antenna
b minimum transmitted power of dipole RFID on AMC plane

doi: 10.1049/iet-map.2012.0685

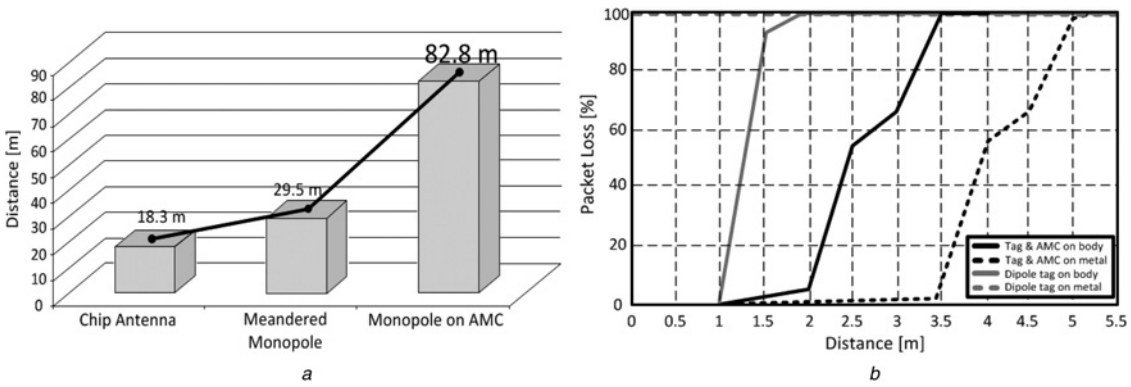

Fig. 8 *Inkjet-printed meandered monopole antenna it was 29.5 m; and with the proposed antenna*

a Communication range of monopole antenna
b read range of RFID on inkjet-printed AMC

3.2 Inkjet-printed SIW

In this section, inkjet-printed SIW on a paper substrate is discussed. SIW structures are similar to conventional dielectric-filled rectangular waveguides using two metallised rows of vias [30]. Microstrip devices are not efficient for high-frequency applications because the short wavelength of the high frequency has tight fabrication tolerance. SIW structures can be considered as a transition between microstrip and dielectric-filled waveguide which has the advantages of both. SIW technology is an emerging approach for the microwave and millimetre-wave components in planar form which allows the integration of components on the same substrate including passive and active components [30]. Realisation of SIW components on paper substrate using inkjet-printing technology has many advantages over conventional SIW technology. The cost can be reduced by introducing inkjet-printed SIW on paper. It allows for arbitrary geometry, and conformal shapes. To be specific, paper substrate enhances the advantages of SIW components such as flexibility, and environmentally-friendly properties. Moreover, the possibility of multi-layered configurations enables reduction in the size of the components.

Simple straight SIW on paper has been designed and fabricated as a first step by Moro *et al.* [31]. Geometry and fabricated SIW structure is shown in Fig. 9. It has been designed for operation frequency of 5 GHz, and its cut-off frequency of the fundamental mode (f_0) is 3.65 GHz. To achieve this performance, the width (w) of the SIW is 23.2 mm, the diameter of vias (d) is 0.8 mm and their pitch (p) spacing is 1.0 mm. For the via metallisation, there are many methods for via hole metallisation such as electroplating and sputtering [32, 33]. However, it is challenging to apply those technique on the paper substrate because those technologies were developed for silicon-based substrates. There was a reported inkjet-printed via hole but the substrate thickness was very thin ($\sim$500 nm) [34]. Many metallisation methods for paper substrate using electroless plating [35] or solder pump technology [36] are under study in order to overcome those challenges. In this paper, for the ease of fabrication, the via holes are made using mechanical drill, and cylindrical copper rivets, with diameter of 0.8 mm, are inserted to metallise the via holes. For the substrate, three layers of paper are stacked which result in the substrate thickness of 0.69 mm. This thickness has been chosen in order to minimise a conductor loss by increasing the substrate thickness since the inkjet-printed silver trace has relatively low conductivity [30]. The scattering parameters such as S_{11} and S_{21} are simulated and measured (Fig. 10). The simulations and measurements agree very well. The high insertion loss above 7 GHz is because of relatively high loss of the substrate at high frequency. This result suggests the possibility of many other inkjet-printed SIW applications on paper such as cavity filter, ridge substrate integrated slab waveguide and antenna in the future.

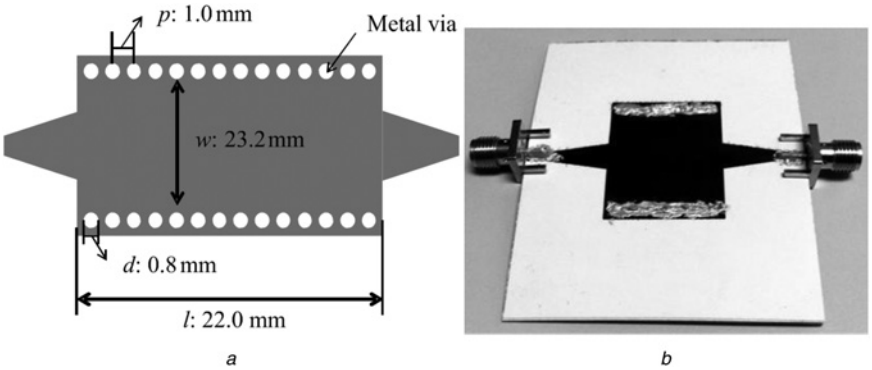

Fig. 9 *Geometry and fabricated SIW structure*

a Geometry and
b fabricated inkjet-printed SIW interconnect on paper

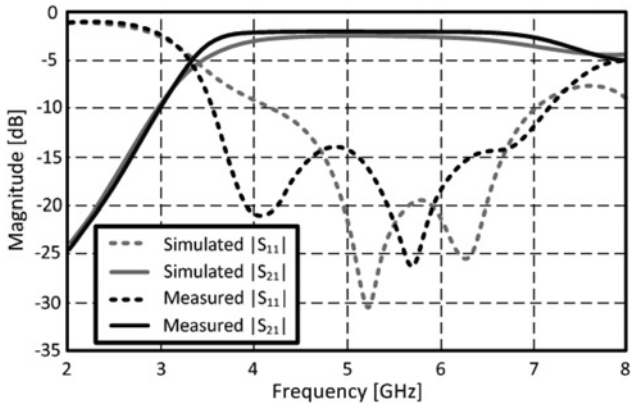

Fig. 10 *Scattering parameters of the SIW on paper*

3.3 Inkjet-printed ambient wireless power scavenging device

In addition to passive microwave components, inkjet printing has also been applied to implement a wireless power scavenging platform. It utilises the ambient RF power found in the existing wireless spectrum to power up a wireless node (mote), including microcontroller and transceiver. Available ambient RF power source was observed in the frequency band between 470 and 570 MHz based on wireless spectrum measurements in Tokyo, Japan. This ultra-high-frequency (UHF) band has not only good propagation characteristics in terms of low attenuation but also low parasitic loss through circuit owing to its long wavelength.

Most current microcontrollers and transceivers have an operating voltage range of between 1.8 and 3.6 V. A low leakage super capacitor charged with wireless power is integrated with the wireless mote in order to avoid usage of a battery. The super capacitors have many advantages over batteries such as higher number of recharge cycle, low leakage and low cost although it has unregulated voltage. The lack of controlling the charge–discharge mechanism of the capacitor may cause the devices to undergo unnecessary power-on-rest (POR). In this case, the micro-controller unit (MCU) will be turned on when the capacitor reached to operation voltage of the MCU causing the capacitor to discharge. Without sufficient power margin, the MCU is going to be shut down before it complete its firmware

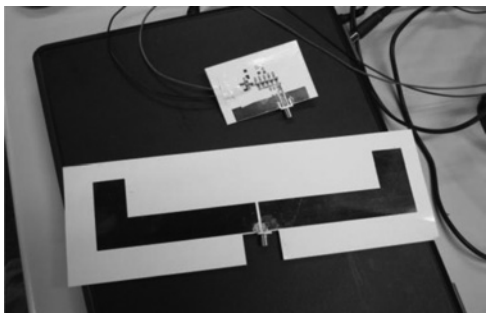

Fig. 11 *Inkjet-printed Ambient wireless power scavenging device*

routine due to insufficient power. There is always a risk of the MCU entering a state of constant PORs without finishing its functioning when the capacitors are utilised as a power storage devices instead of battery. Such a state can be prevented by introducing power management unit (PMU) which is a kind of a switch. It sets a voltage sufficiently higher than the turn-on voltage of the MCU but lower than the maximum operating voltage. The discharge time of the capacitor is the operating time of the device from the PMU triggered turn-on voltage to the turn off voltage of the MCU at 1.8 V [37].

A multi-stage RF voltage multiplier has been used to transform the UHF band RF power to the required voltage of 1.8 V. The proposed charge pump circuit consisted of RF Schottky diodes because of their lower forward voltage drop. It is open circuit to the antenna if the voltage difference across the antenna terminal is lower than the diode's forward voltage drop which results in reflecting back of the wireless power without turning on the device [38]. Therefore, a properly designed RF charge pump circuit was matched to the antenna in order to transform the harvested wireless power to DC voltage, enabling a trickle charge into the end capacitor. The inkjet-printed prototype on paper for power scavenging application is shown in Fig. 11 (Vyas *et al.*). Only 35 μW in free space is enough to generate 1.8 V at its output super capacitor. Also, its input impedance over the frequency of interest is shown (Fig. 12). It has low series dissipative loss ($< 1.1\ \Omega$) and capacitive reactance at its input terminal. An output voltage of 1.8 V is high enough to turn on most current MCUs and wireless transceivers. This experiment has been carried out

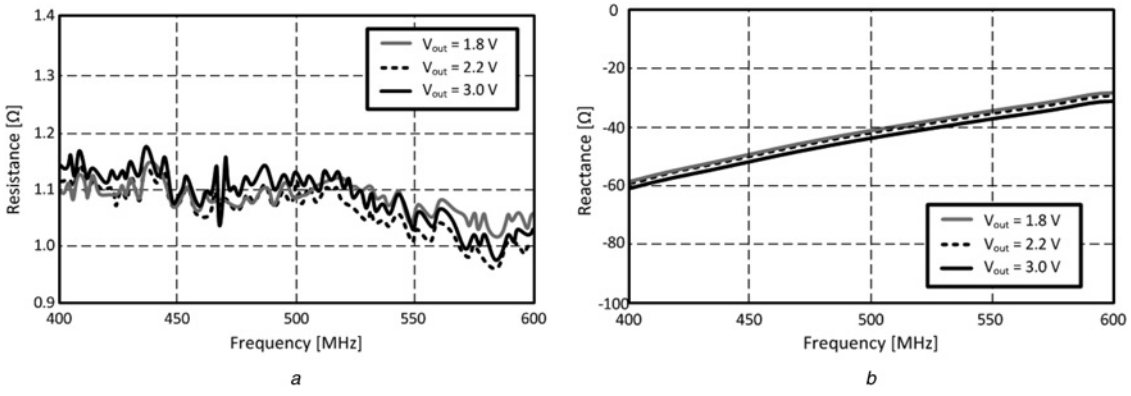

Fig. 12 *Input impedance of the ambient power scavenging device*

a Resistance
b Reactance

doi: 10.1049/iet-map.2012.0685

in Tokyo, Japan. The experiment place was about 6.5 km away from a TV tower.

3.4 Inkjet-printed beacon oscillator on paper substrate

One of the most recent progresses in inkjet-printing technology is implementation of system-level inkjet-printed devices. The system-level implementation of active circuits on flexible substrates has lots of challenges [39]. For these reasons, most of the inkjet-printing works are focused on implementation of single devices such as antennas, inductors and waveguides [1, 3, 7]. The goal of this work is to integrate an active circuit with energy harvesting technology using solar cell by taking advantages of flexible low-cost paper substrate and inkjet-printing technology.

The proposed beacon oscillator operates at 858 MHz. It is powered enough to continuously transmit power or identification information. Such circuits can be used as beacon signal generators or a solar-to-RF power converter in wireless power transmission applications. The operation frequency of this inkjet-printed active antenna can be scaled up or down to any other frequency band depending on its application. Based on the previous designs [40, 41], an inkjet-printed active antenna on flexible paper substrate is designed as shown in Fig. 13 (Kim *et al.* [42]). Tr1 is a JFET, C1–C3 are capacitors, L1–L2 are inductors and R1 is a resistor. The circuit foot print and fabricated prototype are shown in Figs. 13*a* and *b*. The oscillator using a JFET is implemented on inkjet-printed circuit footprint. Oscillation frequency of the proposed active antenna is verified by measuring power spectrum (Fig. 13*c*). And its oscillation quality can be defined by measuring its phase noise. The inkjet-printed circuit has stable oscillation frequency because it has very low phase noise of about -130 dBc/Hz with a power supply at 1 MHz away from carrier frequency (Fig. 13*d*).

3.5 Inkjet-printed nanocarbon-based (graphene and CNTs) gas-sensing technology

Carbon nanomaterials are a very promising area of research for electrical devices. These materials are composed of nanostructured carbon in either cylindrical (SWCNT/MWCNT), or planar (graphene) geometry. Both types of nanocarbon material offer unique electrical, thermal and mechanical properties which make them desirable as potential candidates for the development of next generation electronic devices. Especially, graphene has a lot of promising properties, including high electron mobility (2×10^5 cm^{2}V^{-1}s^{-1}) and high thermal conductivity ($\sim 5 \times 10^3$ Wm^{-1}K^{-1}). Notable properties of graphene for sensor application are its high electrical conductivity and low charge carrier density which result in high sensitivity. Sensitivity can be defined as the change of the sensing material's impedance in the presence of the test gas relative to air, over that of air

$$S = \frac{Z_{\text{gas}} - Z_{\text{air}}}{Z_{\text{air}}} \tag{8}$$

where Z_{air} is impedance of the material in the air and Z_{gas} is impedance of the material in the presence of the test gas. The impedance is a complex impedance (resistance and reactance) of the CNTs at the measuring frequency.

3.5.1 Inkjet-printed CNTs for gas sensing: The first example is the inkjet-printed multi-walled CNT (MWCNT) for sensing applications on paper substrates. A nanostructure for sensing was created using inkjet-printed water-based MWCNT ink. MWCNT was printed on a microstrip lines to test the inkjet-printed sensing material, and target sensing gases like NO_2 and NH_3 were released in certain concentration. A 10 ppm of NO_2 gas resulted in

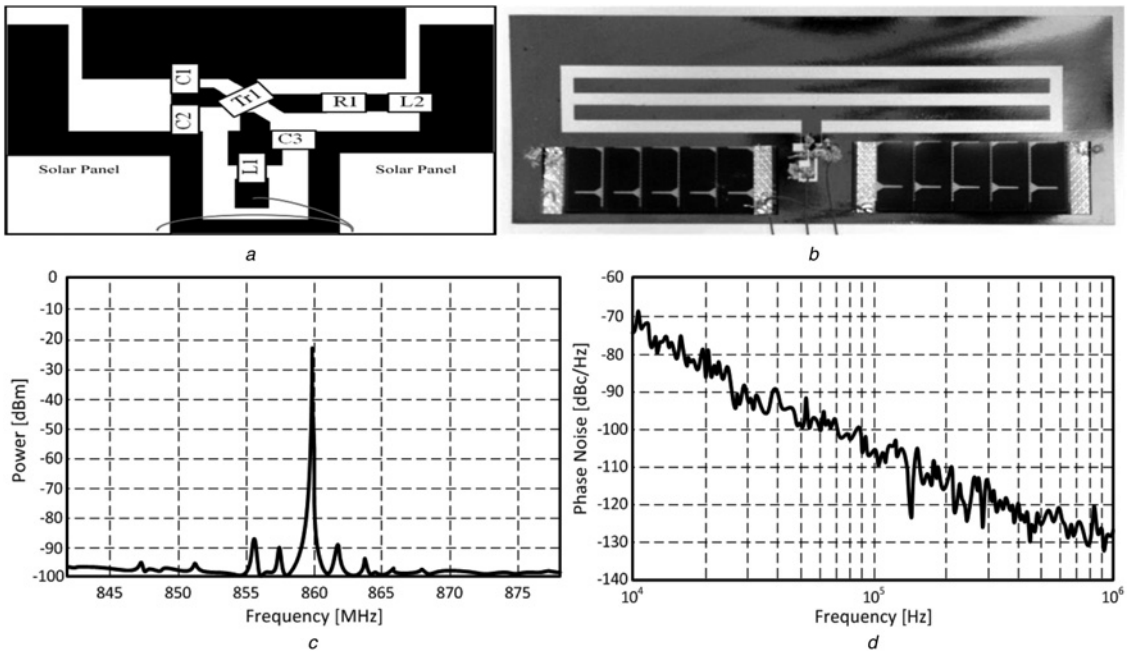

Fig. 13 *Inkjet-printed active antenna on flexible paper substrate is designed*

a Circuit geometry
b Circuit schematic
c Measured spectrum
d Measured phase noise

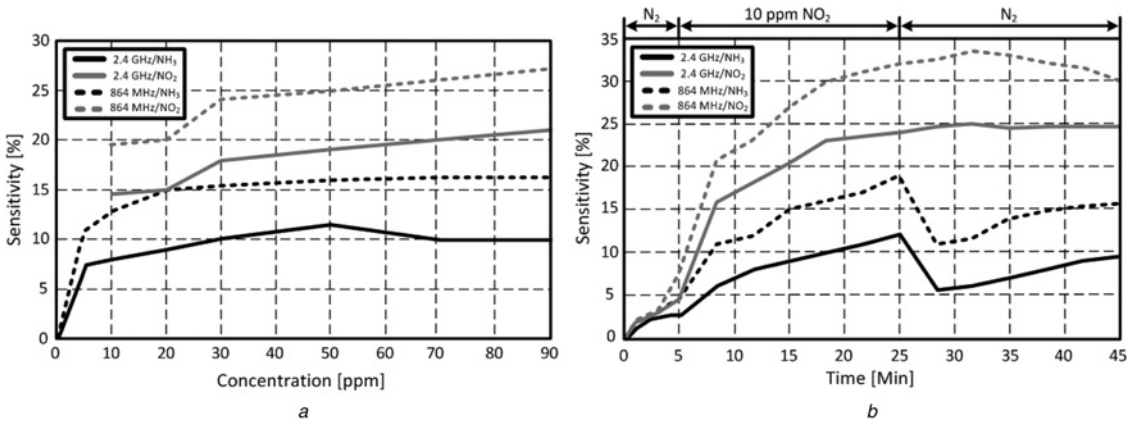

Fig. 14 *Microstrip lines to test the inkjet-printed sensing material, and target sensing gases like NO_2 and NH_3*

a Response of CNTs as a function of concentration after stabilisation
b Timing response of CNTs for NH_3 and NO_2 using concentration of 10 ppm at 864 MHz and 2.4 GHz

sensitivity of 21.7%, and 4 ppm of NH_3 gas resulted in that of 9.4% at 864 MHz (Fig. 14*a*). The sensitivity variation over the time is also presented (Fig. 14*b*). The small increment of sensitivity after shutting down NO_2 is because there are small amount of NO_2 gas remaining in the closed gas chamber for short period. It shows that inkjet-printed MWCNT-based gas sensor has very fast response after gas exposure [43].

3.5.2 Inkjet-printed graphene for gas sensing: In this section, graphene was considered as a sensing material. The first step in the development process was the creation of stable, long-life, inkjet-printable graphene-based inks. This was accomplished by first converting the graphene into graphene oxide (GO) powder. Unlike pristine graphene, which has very poor dispersion in common solvents, GO exhibits excellent solubility in water because of the existence of hydrophilic functional groups on the surface [44], rendering it an excellent candidate for the development of environmental-friendly water-based inks. After deposition, pure graphene can be obtained by the reduction process of GO. The reduction of GO is considered as one of the most promising methods for low-cost, high-yield and scalable preparation of graphene materials [45]. The GO was produced by chemical oxidation of graphite, which introduces oxygen-containing functional groups to exfoliate pristine graphite into individual GO sheets.

A Dimatix Materials Printer (DMP-2800) Series material deposition system was utilised to print both the GO inks. Before printing, the kapton substrate was treated by UV-ozone to improve its hydrophilicity. After printing and curing, printed samples were reduced to obtain the graphene from the GO. A kapton (polyimide) substrate was chosen because of the reduction process of GO which occurs at high temperature. Reduction was achieved by placing the printed GO thin films in elevated temperature in a hydrogen and argon atmosphere. The samples were reduced at 200°C for 30 min and 300°C for another 30 min. The heating rate was 5°C/min. After reduction, the samples were left to cool down to room temperature naturally.

Tao *et al.* reported the experimental results of inkjet-printed graphene for gas sensing [46–48]. The results of 500 ppm NH_3 gas testing are measured, and the dimensions of pattern 1 are 1 mm × 1 mm, pattern 2 is 1 mm × 2 mm and pattern 3 is 1 mm × 3 mm (Figs. 15*a* and *b*). The inkjet-printed reduced graphene oxide (RGO) thin films of different dimensions show similar responses to 500 ppm NH_3. The electrical resistance rapidly increases in the first few minutes after the introduction of NH_3, indicating a fast detection rate. With the continued supply of NH_3, the resistance change begins to diminish after 10 min, which

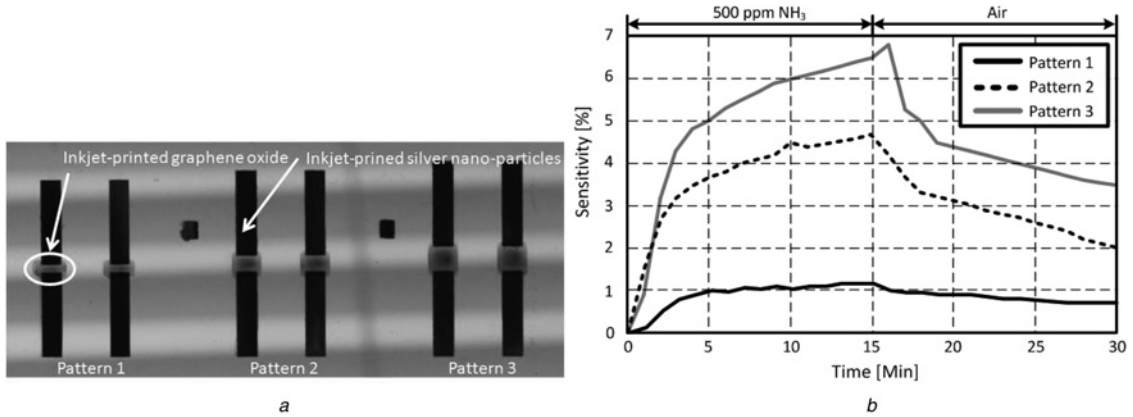

Fig. 15 *Experimental results of inkjet-printed graphene for gas sensing*

a Inkjet-printed GO on kapton
b Measured response of RGO thin films to 500 ppm NH_3

doi: 10.1049/iet-map.2012.0685

occurs as the material enters the saturation region. The maximum sensitivity is observed in the case of pattern 3, which shows greater than 6% increase in normalised resistance. After the introduction of NH_3, air was introduced into the system and it was found that the resistance quickly recovered a large portion of its original value ($\sim$30%) within 5 min.

Compared to other works on graphene-based gas sensors, the proposed inkjet-printed RGO demonstrates superior performance, including a high sensitivity, fast response and quick recovery. Particularly, the short recovery time in natural environmental conditions is advantageous over other recovery methods which used UV and heat treatment to assist the recovery, and is of great importance for practical applications [49]. The sensor exhibits an observable ($\sim$10 Ω) change in resistance within one minute after introducing NH_3, a measure which is certainly in the detectable range of the backend circuitry of the WISP platform.

4 Future works

Significant amounts of research have been done in the area of inkjet-printed microwave devices and components in recent years. Yet, there is still significant amount of research to be done. It is necessary to find ways to overcome challenges of inkjet-printed electronics in order to maximise its advantages. One of the most significant issues is to improve the durability of the inkjet-printed electronics on paper substrates since inkjet-printed silver patterns on paper substrate are very sensitive to the surrounding environment. Moisture in the surrounding environment has a significant effect on the inkjet-printed electronics on the paper because the paper tends to absorb water vapours which results in malfunctioning of the inkjet-printed electronics. A special chemical such as Parylene can be utilised to protect inkjet-printed electronics from harmful elements in the environment. The Parylene is very stable, biocompatible and a conformal material, which is compatible with inkjet-printing technology [50]. Realising the waterproof inkjet-printed electronics on flexible substrate is a critical factor for implementing washable inkjet-printed electronics on flexible substrates such as paper and fabric.

Next, the successful implementation of inkjet-printed microwave structures on paper substrate such as inkjet-printed AMC structures, RF power scavenging circuit and SIW suggest the latent possibility of the inkjet-printing technology for microwave applications. First of all, the inkjet-printed AMC structures can be integrated to improve the performance of conventional microwave devices. Antennas for RFID application are good examples for the application of the inkjet-printed AMC structures. The proposed designs can be applied to UHF RFID frequency band (915 MHz) by miniaturising the unit cell of the AMC structure which enables the realisation of low-cost compact inkjet-printed RFID tag for wearable or on-metal application. In addition, it is possible to implement a compact reconfigurable microwave device by taking advantage of the flexible paper substrate and inkjet-printing technology. The inkjet-printed electronics on paper substrate can be folded without damaging electrical performance when a concept of origami is introduced. A horn antenna or a reflector of reflector-type antenna can be folded or expanded easily due to flexibility of the paper and its ease of process. For the SIW components, there are a lot of applications such as filters and antennas that can be implemented based on the results of inkjet-printed SIW on the paper because the simple microstrip-to-SIW transition has been successfully realised, which is the basic of any other SIW-based components and devices.

Another promising progress in inkjet printing area is feasibility of sensing gases using nanocarbon structures such as CNTs and graphene. It implies that the boarder of inkjet-printing technology has been broadened to nanotechnology, which enables clean-room-like processes without the need for a clean-room or use of high cost equipments for handling nanostructures. It suggests the implementation feasibility of the low-cost high-sensitive gas-detecting system using nanocarbon structures. Moreover, this technology can be applied to biomedical areas to detect proteins by inkjet-printing biomedical sensing materials like cells or enzymes.

5 Conclusion

This paper has presented the state-of-the-art of inkjet-printing technology for microwave area: the recent advances in the field of passive/active components, system-level circuit integration and nanocarbon-based sensing in inkjet-printing technology have been described and discussed. Issues related to the design of the inkjet-printed components and circuits have been discussed, and the experimental results of the discussed inkjet-printed devices are presented. Future works are also discussed based on the state-of-the-art results of inkjet-printing technology.

6 Acknowledgments

The work of A. Georgiadis and A. Collado was supported by EU Marie Curie FP7-PEOPLE-2009-IAPP 251557, the Spanish Ministry of Economy and Competitiveness project TEC2012-39143. The work of S. Kim, B. Cook, T. Le, J. Cooper, H. Lee, V. Lakafosis, R. Vyas and M. M. Tentzeris was supported by NSF, NEDO and IFC/SRC.

7 References

1 Mager, D., Peter, A., Del Tin, L., *et al.*: 'An MRI receiver coil produced by inkjet printing directly on to a flexible substrate', *IEEE Trans. Imag.*, 2010, **29**, (2), pp. 482–487
2 Basiricò, L., Cosseddu, P., Fraboni, B., Bonfiglio, A.: 'Inkjet printing of transparent, flexible, organic transistors', *Thin Solid Films*, 2011, **520**, (4), pp. 1291–1294
3 Rida, A., Yang, L., Vyas, R., Tentzeris, M.M.: 'Conductive inkjet-printed antennas on flexible low-cost paper-based substrates for RFID and WSN applications', *IEEE Antenna Propag. Mag.*, 2009, **51**, (3), pp. 13–23
4 Yang, L., Tentzeris, M.M.: 'Design and characterization of novel paper-based inkjet-printed RFID and microwave structures for telecommunication and sensing applications'. IEEE MTT-S Int. Microwave Symp. Digest, 2007, pp. 1633–1636
5 Mishima, T., Tanaka, K., Abe, N., Taki, H.: 'Toward construction of a mobile system with long-range RFID sensors'. Proc. IEEE Cybernetics Intelligent System Conf., 2004, vol. 2, pp. 960–965
6 Vyas, R., Lakafosis, V., Lee, H., *et al.*: 'Inkjet printed, self -powered, wireless sensors for environmental, gas, and authentication-based sensing', *IEEE Sens. J.*, 2011, **11**, (12), pp. 3139–3152
7 Yang, L., Rida, A., Vyas, R., Tentzeris, M.M.: 'RFID tag and RF structures on a paper substrate using inkjet-printing technology', *IEEE Trans. Microw. Theory Techn.*, 2007, **MTT 55**, (12), pp. 2894–2901
8 Lakafosis, V., Rida, A., Vyas, R., Li, Y., Nikolaou, S., Tentzeris, M.M.: 'Progress towards the first wireless sensor networks consisting of inkjet-printed, paper-based RFID-enabled sensor tags', *Proc. IEEE*, 2010, **98**, (9), pp. 1601–1609

9 Yi, L., Torah, R., Beeby, S., Tudor, J.: 'An all-inkjet printed flexible capacitor for wearable applications'. 2012 Symp. Design, Test, Integration and Packaging of MEMS/MOEMS (DTIP), 2012, pp. 192–195

10 Maekawa, K., Yamasaki, K., Niizeki, T., *et al.*: 'Drop-on-demand laser sintering with silver nanoparticles for electronics packaging', *IEEE Trans. Compon. Pack. Manuf. Technol.*, 2012, **2**, (5), pp. 868–877

11 Polzinger, B., Schoen, F., Matic, V., *et al.*: 'UV-sintering of inkjet-printed conductive silver tracks'. 2011 11th IEEE Conf. on Nanotechnology (IEEE-NANO), 2011, pp. 201–204

12 Allen, M., Alastalo, A., Suhonen, M., Mattila, T., Leppäniemi, J., Seppa, H.: 'Contactless electrical sintering of silver nanoparticles on flexible substrates', *IEEE Trans. Microw. Theory Techn.*, 2011, **59**, (5), pp. 1419–1429

13 Cook, B.S., Shamim, A.: 'Inkjet printing of novel wideband and high gain antennas on low-cost paper substrate', *IEEE Trans. Antenna Propag.*, 2012, **60**, (9), pp. 4148–4156

14 Caglar, U., Kaija, K., Mansikkamäki, P.: 'Analysis of mechanical performance of silver inkjet-printed structures'. Second IEEE Int. Nanoelectronics Conf. 2008 (INEC 2008), 2008, pp. 851–856

15 Thompson, D.C., Tantot, O., Jallageas, H., Ponchak, G.E., Tentzeris, M. M., Papapolymerou, J.: 'Characterization of liquid crystal polymer (LCP) material and transmission lines on LCP substrates from 30 to 110 GHz', *IEEE Trans. Microw. Theory Techn.*, 2004, **MTT 52**, (4), pp. 1343–1352

16 Latti, K.P., Kettunen, M., Strom, J.P., Silventoinen, P.: 'A review of microstrip T-resonator method in determining the dielectric properties of printed circuit board materials', *IEEE Trans. Instrum. Meas.*, 2007, **56**, (5), pp. 1845–1850

17 Chang, K., Hsieh, L.-H.: 'Microwave ring circuits and related structures' (Wiley, 2004)

18 Fulford, A.R., Wentworth, S.M.: 'Conductor and dielectric-property extraction using microstrip tee resonators', *Microw. Optic. Technol. Lett.*, 2005, **47**, pp. 14–16

19 Shaker, G., Safavi-Naeini, S., Sangary, N., Tentzeris, M.M.: 'Inkjet printing of ultrawideband (UWB) antennas on paper-based substrates', *IEEE Antennas Wirel. Propag. Lett.*, 2011, **10**, pp. 111–114

20 Parker, E.A., Hamdy, S.M.A.: 'Rings as elements for frequency selective surfaces', *Electron. Lett.*, 1981, **17**, pp. 612–614

21 Parker, E.A., El Sheikh, A.N.A.: 'Convoluted array elements and reduced size unit cells for frequency-selective surfaces', *Proc. Inst. Electr. Eng. H, Microw. Antennas Propag.*, 1991, **138**, pp. 19–22

22 Shung-Wu, L., Zarrillo, G., Chak-Lam, L.: 'Simple formulas for transmission through periodic metal grids or plates', *IEEE Trans. Antennas Propag.*, 1982, **30**, pp. 904–909

23 Shaker, G., Lee, H., Duncan, K., Tentzeris, M.: 'Integrated antenna with inkjet-printed compact artificial magnetic surface for UHF applications'. 2010 IEEE Int. Conf. on Wireless Information Technology and Systems (ICWITS), 2010, pp. 1–4

24 Sievenpiper, D., Broas, R., Yablonovitch, E.: 'Antennas on high-impedance ground planes', *IEEE MTT-S Int. Microw. Symp. Dig.*, 1999, **3**, pp. 1245–1248

25 Kim, S., Ren, Y.J., Lee, H., Rida, A., Nikolaou, S., Tentzeris, M.M.: 'Monopole antenna with inkjet-printed EBG array on paper substrate for wearable applications', *IEEE Antennas Wirel. Propag. Lett.*, 2012, **11**, pp. 663–666

26 Cure, D., Weller, T., Miranda, F.: 'A comparison between Jerusalem cross and square patch frequency selective surfaces for low profile antenna applications'. Proc. 2011 Int. Conf. on Electromagnetics in Advanced Applications (ICEAA), 2011, pp. 1019–1022

27 Cooper, J.R., Kim, S., Tentzeris, M.M.: 'A novel polarization-independent, free-space, microwave beam splitter utilizing an inkjet-printed, 2-D array frequency selective surface', *IEEE Antennas Wirel. Propag. Lett.*, 2012, **11**, pp. 686–688

28 Lee, H., Kim, S., Donno, D.D., Tentzeris, M.M.: 'A novel "universal" inkjet-printed EBG-backed flexible RFID for rugged on-body and metal mounted applications'. Proc. 2012 IEEE Int. Microwave Symp., 2012, pp. 1–3

29 Kim, S., Tentzeris, M.M., Nikolaou, S.: 'Wearable biomonitoring monopole antennas using inkjet printed electromagnetic band gap structures'. Proc. 2012 Sixth European Conf. on Antennas and Propagation (EUCAP), 2012, pp. 181–184

30 Bozzi, M., Georgiadis, A., Wu, K.: 'Review of substrate-integrated waveguide circuits and antennas', *IET Microw. Antennas Propag.*, 2011, **5**, (8), pp. 909–920

31 Moro, R., Kim, S., Bozzi, M., Tentzeris, M.: 'Novel inkjet-printed substrate integrated waveguide (SIW) structures on low-cost materials for wearable applications'. Proc. 42th European Microwave Conf. 2012 (EuMC 2012), 2012, pp. 72–75

32 Lee, J.Y., Lee, S.K., Park, J.H.: 'Fabrication of void-free copper filled through-glass-via for wafer-level RF MEMS packaging', *Electron. Lett.*, 2013, **48**, (17), pp. 1076–1077

33 Yu, C., Sandhy, G.S., Doan, T.T.: 'The combination of high temperature sputtering with excimer laser planarization for submicrometer contact via filling', *J. Appl. Phys.*, 1992, **72**, (4), pp. 1599–1607

34 Kawase, T., Sirringhaus, H., Friend, R.H., Shimoda, T.: 'Inkjet printed via-hole interconnections and resistors for all-polymer transistor circuits', *Adv. Mater.*, 2001, **13**, (21), pp. 1601–1605

35 Ohno, I.: 'Electrochemistry of electroless plating', *Mater. Sci. Eng. A*, 1991, **146**, (1), pp. 33–49

36 Gu, J., Pike, W.T., Karl, W.J.: 'Solder pump technology for through-silicon via fabrication', *J. Microelectromech. Syst.*, 2011, **20**, (3), pp. 561–563

37 Vyas, R., Lakafosis, V., Nishimoto, H., Tentzeris, M., Kawahara, Y.: 'A battery-less, wireless mote for scavenging wireless power at UHF (470–570 MHz) frequencies'. IEEE Int. Symp. on Antennas and Propagation and USNC/URSI National Science Meeting, 2011, pp. 1069–1072

38 Vyas, R., Nishimoto, H., Tentzeris, M., Kawahara, Y., Asami, T.: 'A battery-less, wireless mote for scavenging wireless power at UHF (470–570 MHz) frequencies'. IEEE Int. Microwave Symp., 2012, pp. 1069–1072

39 Chang, K., York, R.A., Hall, P.S., Itoh, T.: 'Active integrated antennas', *IEEE Trans. Microw. Theory Techn.*, 2002, **50**, (3), pp. 937–944

40 Giuppi, F., Georgiadis, A., Via, S., *et al.*: 'A 927 MHz solar powered active antenna oscillator beacon signal generator'. 2012 IEEE Topical Conf. on Wireless Sensors and Sensor Networks (WiSNET), 2012, pp. 1–4

41 Georgiadis, A., Collado, A., Kim, S., Lee, H., Tentzeris, M.M.: 'UHF solar powered active oscillator antenna on low cost flexible substrate for application in wireless identification'. IEEE MTT-S IMS, 2012, pp. 1–3

42 Kim, S., Georgiadis, A., Collado, A., Tentzeris, M.M.: 'An inkjet-printed solar-powered wireless beacon on paper for identification and wireless power transmission applications', *IEEE Trans. Microw. Theory Techn.*, 2012, **60**, (12), pp. 4178–4186

43 Mangu, R., Rajaputra, S., Singh, V.P.: 'MWCNT-polymer composites as highly sensitive and selective room temperature gas sensors', *Nanotechnology*, 2011, **21**, pp. 103115–1031153

44 Lin, Z., Yao, Y., Li, Z., Liu, Y., Li, Z., Wong, C.-P.: 'Solvent-assisted thermal reduction of graphite oxide', *J. Phys. Chem. C*, 2010, **114**, (35), pp. 14819–14825

45 Li, Z., Yao, Y., Lin, Z., Moon, K.-S., Lin, W., Wong, C.P.: 'Ultrafast, dry microwave synthesis of graphene sheets', *J. Mater. Chem.*, 2010, **20**, pp. 4781–4783

46 Le, T., Thai, T., Lakafosis, V., *et al.*: 'Graphene enhanced wireless sensors'. IEEE Sensors, 2012

47 Le, T., Lakafosis, V., Lin, Z., Wong, C.P., Tentzeris, M.M.: 'Inkjet-printed graphene-based wireless gas sensor modules'. 2012 IEEE 62nd Electronic Components and Technology Conf. (ECTC), 2012, pp. 1003–1008

48 Le, T., Lakafosis, V., Thai, T., Lin, Z., Tentzeris, M.: 'Inkjet printing of graphene thin films for wireless sensing applications'. 2012 Int. Conf. on Electromagnetics in Advanced Applications (ICEAA), September 2012, pp. 954–957

49 Schedin, F., Geim, A.K., Morozov, S.V., *et al.*: 'Detection of individual gas molecules adsorbed on grapheme', *Nat. Mater.*, 2007, **6**, pp. 652–655

50 Sharifi, H., Lahiji, R.R., Han-Chung, L., Ye, P.D., Katehi, L.P.B., Mohammadi, S.: 'Characterization of Parylene-N as flexible substrate and passivation layer for microwave and millimeter-wave integrated circuits', *IEEE Trans. Adv. Pack.*, 2009, **32**, pp. 84–92

doi: 10.1049/iet-map.2012.0685